Voltage sensor movements of $Ca_V1.1$ during an action potential in skeletal muscle fibers

Quinton Banks[a,1], Hugo Bibollet[a,1], Minerva Contreras[a], Daniel F. Bennett[b], Roger A. Bannister[a,b], Martin F. Schneider[a,2], and Erick O. Hernández-Ochoa[a,2]

[a]Department of Biochemistry and Molecular Biology, University of Maryland School of Medicine, Baltimore, MD 21201; and [b]Department of Pathology, University of Maryland School of Medicine, Baltimore, MD 21201

Edited by Francisco Bezanilla, University of Chicago, Chicago, IL, and approved August 24, 2021 (received for review December 30, 2020)

The skeletal muscle L-type Ca^{2+} channel ($Ca_V1.1$) works primarily as a voltage sensor for skeletal muscle action potential (AP)-evoked Ca^{2+} release. $Ca_V1.1$ contains four distinct voltage-sensing domains (VSDs), yet the contribution of each VSD to AP-evoked Ca^{2+} release remains unknown. To investigate the role of VSDs in excitation–contraction coupling (ECC), we encoded cysteine substitutions on each S4 voltage-sensing segment of $Ca_V1.1$, expressed each construct via in vivo gene transfer electroporation, and used *in cellulo* AP fluorometry to track the movement of each $Ca_V1.1$ VSD in skeletal muscle fibers. We first provide electrical measurements of $Ca_V1.1$ voltage sensor charge movement in response to an AP waveform. Then we characterize the fluorescently labeled channels' VSD fluorescence signal responses to an AP and compare them with the waveforms of the electrically measured charge movement, the optically measured free myoplasmic Ca^{2+}, and the calculated rate of Ca^{2+} release from the sarcoplasmic reticulum for an AP, the physiological signal for skeletal muscle fiber activation. A considerable fraction of the fluorescence signal for each VSD occurred after the time of peak Ca^{2+} release, and even more occurred after the earlier peak of electrically measured charge movement during an AP, and thus could not directly reflect activation of Ca^{2+} release or charge movement, respectively. However, a sizable fraction of the fluorometric signals for VSDs I, II, and IV, but not VSDIII, overlap the rising phase of charge moved, and even more for Ca^{2+} release, and thus could be involved in voltage sensor rearrangements or Ca^{2+} release activation.

action potential | $Ca_V1.1$ | voltage sensor domain | excitation–contraction coupling | skeletal muscle

During membrane depolarization of a skeletal muscle fiber, L-type Ca^{2+} channels ($Ca_V1.1$) in the transverse-tubule (TT) membrane serve as voltage-sensors for activation of Ca^{2+} release (1, 2) from the adjacent but structurally distinct sarcoplasmic reticulum (SR) via ryanodine receptor type-1 (RyR1) Ca^{2+} release channels in the SR terminal cisternae (3, 4). This series of events is known as excitation–contraction coupling (ECC) of skeletal muscle (5). Translocation of the voltage-sensing domains (VSDs) is also coupled to opening of $Ca_V1.1$ channel permeation pore in $Ca_V1.1$, which mediate inward Ca^{2+} current across the TT membrane (6). However, the L-type current is relatively small and slowly activating, and numerous reports indicate that $Ca_V1.1$ Ca^{2+} current may play little or no role in the events that initiate ECC (7–9). Although the role of $Ca_V1.1$ functioning as the voltage sensor for SR Ca^{2+} release in ECC has been clearly established, many aspects of how the $Ca_V1.1$ works as a voltage sensor during muscle fiber activation remain unknown. Surprisingly, the voltage-sensor movements during an action potential (AP), which is the physiological stimulus for the muscle fiber activation (10), have not been previously measured in muscle or in any other cell type.

The skeletal muscle voltage-gated L-type Ca^{2+} channel is a heteromultimeric protein composed of a voltage-sensor and pore-forming α_{1S} subunit ($Ca_V1.1$), and auxiliary subunits β1a, α2δ1, and γ (11, 12). $Ca_V1.1$ contains four homologous domains (I to IV) (Fig. 1*A*). Each repeat is comprised of six (S1 to S6) transmembranal helical segments; the VSD is formed by the S1 to S4 segments, and the pore domain is formed by spanning helices S5 and S6 (Fig. 1*A*) (12, 13). The S4 segment in each VSD contains positively charged Arg or Lys (Fig. 1 *A* and *B*), a conserved motif across the family of voltage-gated channels, that undergoes conformational changes in response to membrane depolarization and it is thought to be the primary voltage-sensing region (14–17). Each $Ca_V1.1$ is composed of a central pore and four highly similar but distinct heterogenous VSD (VSD I–IV) in the three-dimensional space (Fig. 1*C*) (12). Because in other voltage-gated channels individual VSDs appear to be differentially involved in specific aspects of channel gating (18–21), here we hypothesized that not all the VSDs in $Ca_V1.1$ contribute equally to ECC. Intramembrane movements of $Ca_V1.1$ VSDs I–IV within the TTs during fiber depolarization generate a small electrical current (2), but neither the charge movement during the AP nor the contribution of the individual VSDs to voltage-gated Ca^{2+} release has been previously monitored.

Here, we introduce a two-pronged approach to monitoring movement of VSD charges during an AP in adult muscle fibers. First, we electrically monitored the total VSD charge moved during a muscle AP using the AP voltage-clamp (APVC) technique, applied here to skeletal muscle fibers. Next, we introduce AP-fluorometry, a variant of the voltage-clamp fluorometry (VCF) (22), to optically track the movement of each VSD via a cysteine (Cys) substitution on the extracellular flank of the S4 of each VSD

Significance

A continuously evolving question regarding excitation–contraction coupling (ECC) in skeletal muscle has been around the mechanism that links the activation of the $Ca_V1.1$ voltage sensor with the intracellular Ca^{2+} release. $Ca_V1.1$ senses changes in transmembranal voltage through four distinct voltage-sensing domains (VSDs I–IV), yet whether one or all contribute to ECC is unknown. To investigate the roles of each VSD, this work introduces AP fluorometry to track conformational changes of $Ca_V1.1$ voltage sensors and AP voltage clamp to measure the charge movement during an AP waveform in muscle fibers. The rising phase of the fluorescence signals from VSDs I, II, and IV were faster than that of VSDIII, suggesting a differential contribution of VSD movements to ECC.

Author contributions: M.F.S. and E.O.H.-O. designed research; Q.B., H.B., M.C., D.F.B., R.A.B., and E.O.H.-O. performed research; M.C. and D.F.B. contributed new reagents/analytic tools; Q.B., H.B., and E.O.H.-O. analyzed data; and M.F.S. and E.O.H.-O. wrote the paper.

The authors declare no competing interest.

This article is a PNAS Direct Submission.

[1]Q.B. and H.B. contributed equally to this work.

[2]To whom correspondence may be addressed. Email: MSchneid@som.umaryland.edu or ehernandez-ochoa@som.umaryland.edu.

This article contains supporting information online at https://www.pnas.org/lookup/suppl/doi:10.1073/pnas.2026116118/-/DCSupplemental.

Published September 28, 2021.

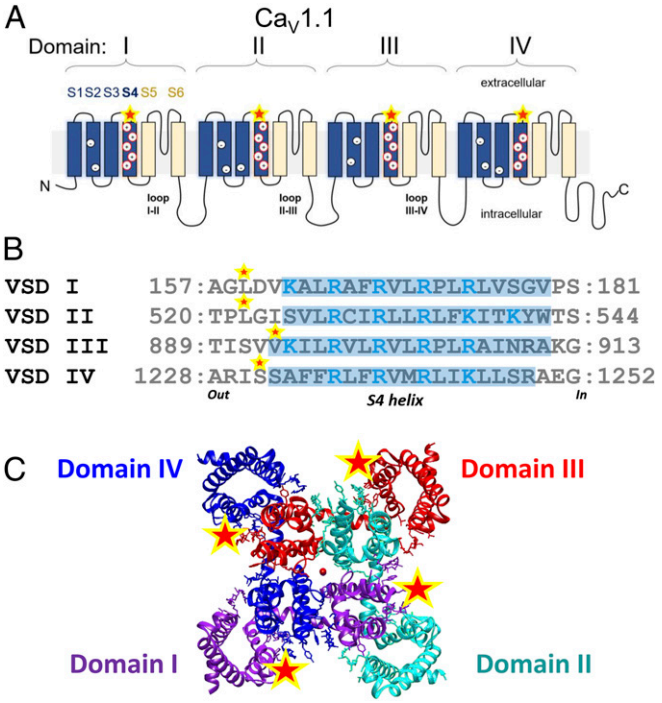

Fig. 1. $Ca_V1.1$ membrane topology, VSDs S4 helix comparisons and structure. (*A*) Membrane topology of the $Ca_V1.1$ α1 subunit. The α1 subunit is composed by four homologous (but not identical) domains, consisting of six transmembrane domains, S1 to S6. S1 to S4 from each domain form a VSD, whereas S5 and S6 from all four domains form the pore domain. Intracellular loops connect the domains, the loops II-III and I-II are important for ECC. (*B*) Sequence alignment of VSDI to -IV of $Ca_V1.1$. Arg and Lys within S4 helices proposed critical for voltage sensing are highlighted in blue. Residues substituted by Cys for fluorescent labeling (VSDI L159C; VSDII L522C; VSDIII V893C; VSDIV S1231C) are indicated (star). (*C*) Extracellular view of cryoelectron microscopy reconstruction of $Ca_V1.1$ α1 subunits (domain I, green; domain II, cyan; domain III, red; and domain IV, blue) with relative location of mutation points marked (star) and calcium ions in the pore (central red dot). S4 helix delimitation is indicated with light blue highlight based on the cryoelectron microscopy structure and the rabbit $Ca_V1.1$ sequence (PDB ID code 5GJW and Uniprot ID P07293) (12). Auxiliary subunits (i.e., β1a, α2δ1, γ, and STAC3), important for $Ca_V1.1$ function, are not illustrated.

and its labeling with a cysteine-reacting fluorescent probe, which serves as an optical reporter of local rearrangements in response to an AP. Parallel optical recordings of AP and Ca^{2+} transients, and the calculated Ca^{2+} release rate from SR, were also obtained to establish the temporal correlation between AP, AP-elicited charge movement, AP-evoked Ca^{2+} transient, SR Ca^{2+} release flux, and VSD conformational changes.

Our electrical measurements show that a peak of about 65% of the total available voltage-sensor charge is moved during a single muscle fiber AP. Our optical measurements show that the peak of the detected fluorescence change signals from fluorophores introduced into each of the VSDs occurs about 3 to 7 ms later than the peak of the electrically measured charge movement, indicating that the conformational changes of the fluorophores at the labeled sites is slower than the movement of the VSD charged residues. However, a sizable fraction of the fluorescence signal for VSDs I, II, and IV, but not VSDIII overlap the rising phase of charge moved, and even more for Ca^{2+} release, and thus could be involved in voltage sensor rearrangements or Ca^{2+} release activation.

Results

The properties of the intramembrane charge movement, an early event of ECC, have been characterized primarily using voltage clamp step-like depolarizations (23). Because the physiological stimulus for ECC is an AP, we wanted to characterize the time course of the charge movement evoked by an AP waveform. We first used the two-microelectrode voltage-clamp technique in an APVC command mode (24, 25) with all ionic channel currents blocked (*SI Appendix*) to create an AP voltage time course (Fig. 2*A*, red trace) that very closely mimicked the optically measured AP evoked by field stimulation of other fibers with no channels blocked (Fig. 2*A*, black trace). The voltage clamp could also provide a step voltage change (Fig. 2*A*, blue trace) for reference in each fiber examined by APVC. The optically recorded AP time courses were essentially the same at different locations along the fiber during APVC (Fig. 2*B*), establishing spatial uniformity of the APVC. The total current recorded under APVC conditions was corrected for linear components using P/5 protocol (26) (*SI Appendix*, Figs. S1 and S2), giving the net nonlinear current moved in response to the AP time course (Fig. 2*E*, red trace). During APVC, the voltage sensors initially move outward during the depolarization phase of the AP, giving a positive (outward) phase of nonlinear current (Fig. 2*E*, initial phase of red trace). The positive current is then reversed during and after the AP repolarization, giving a negative (inward) phase of nonlinear current (Fig. 2*E*, later phase of red trace), generated by the return of the voltage sensors to their starting distribution within the membrane. For comparison, the nonlinear current generated in response to the step depolarization (Fig. 2*C*, blue trace) is only outward during the time represented in Fig. 2*E*, since only the depolarizing step of the 20-ms depolarizing pulse is shown.

The net charge moved outward during the depolarization phase of the AP was close to equal to the charge moved back during and after the repolarization phase of the AP (Fig. 2 *F* and *G*), consistent with charge conservation during intramembrane charge movements (2). Compared with the charge moved by the step depolarization to +20 mV (Fig. 2 *D* and *F*, blue trace), which should move the maximum available mobile charge (Q_{max}) (27), the AP moved ~65% of Q_{max} (Fig. 2 *F* and *H*). Comparison of normalized records of the AP and charge movement [$Q(t)$] time courses (Fig. 2*I*) shows that the peak of $Q(t)$ follows the peak of the AP by 1.46 ± 0.17 (mean ± SD) ms. The full duration at half maximum of the $Q(t)$ moved by the AP was 2.59 ± 0.32 ms. Our electrical measurements of charge movement during an AP (Fig. 2*F*) include the sum total of the currents carried by all four of the VSDs of $Ca_V1.1$ (Fig. 1*A*). They represent recordings of voltage-sensor charge movement in response to the AP waveform in any cell type.

Ca^{2+} transients were recorded in other fibers (Fig. 2*I*, gray trace), and used to calculate the rate of release (Rel) of Ca^{2+} from the SR (Fig. 2*I*, dark yellow trace) in response to propagated APs (see *SI Appendix* for details about Rel calculation). The average time to peak of the calculated Rel for the propagated AP (3.37 ± 0.31 ms, $n = 12$) followed the time to peak of $Q(t)$ recorded during APVC in other fibers (Fig. 2*I*).

To examine movements of the individual VSDs, which may be differentially involved in channel gating (21), a Cys was introduced at the extracellular side of the S4 helix in each VSD of the $Ca_V1.1$ α-subunit and expressed in muscle fibers. Fibers were labeled with a Cys-reacting fluorophore (Fig. 1 *B* and *C*), and used for AP fluorometry, a modified version of the VCF (22), here applied to monitor individual VSD movements during an AP in isolated muscle fibers.

We first explored the feasibility of using a $Ca_V1.1$ construct (EGFP-$Ca_V1.1$ L522C) with a single Cys located just proximal to the S4 helix of domain II to monitor S4 movements in adult mouse skeletal muscle fibers. We used the starting cDNA construct EGFP (Enhanced Green Fluorscent Protein)-$Ca_V1.1$ α_{1S}, an N-terminally EGFP-tagged rabbit $Ca_V1.1$ (28, 29). Previous studies have shown that this EGFP-$Ca_V1.1$ fusion protein localizes and functions nearly identically to untagged wild-type

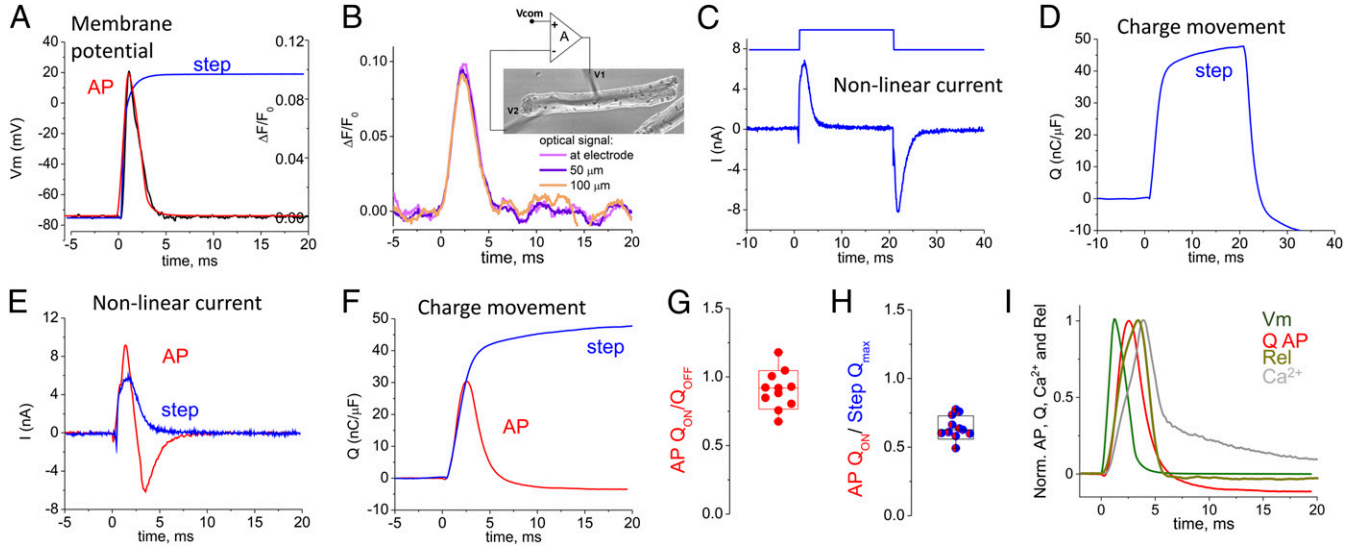

Fig. 2. VSD charge movement during an AP depolarization. (*A*) Optical measurement of propagated AP, black trace; imposed APVC waveform, red trace; step depolarization, blue trace. (*B*) Di-8-ANEPPS signals at varying distances from current injecting electrode (*Inset*) in a muscle fiber. (*C*) Outward and inward nonlinear capacitive currents in response to a voltage step to +20 mV. (*D*) Charge movement trace estimated from *C* in response to voltage step to +20 mV (blue). (*E*) Outward and inward nonlinear capacitive currents in response to the AP waveform and outward current for a voltage step to +20 mV. (*F*) Charge movement traces estimated from *E* in response to AP waveform (red) vs. voltage step to +20 mV (blue). (*G*) Box and whisker plot showing ratio of Q_{ON} to Q_{OFF} for the AP waveform. (*H*) Box and whisker plot showing for Q_{ON} from and AP compared with Q_{max}. Whisker indicate minimum and maximum, box delimitation indicates ±SD. Currents evoked by voltage steps and AP waveform were recorded in the same fibers ($n = 7$). Note the voltage sensor returns to starting position after the AP repolarization but not with step depolarizations. (*I*) Average normalized time course of the AP (green) and charge (Q) moved during an AP (red), and AP evoked fluo-4 Ca^{2+} transient (Ca^{2+}; gray line) and corresponding Ca^{2+} release flux waveform (Rel; dark yellow trace, $n = 12$). All signals were assessed in different sets of fibers. AP, Q, Ca^{2+} transients, and derived Ca^{2+} release flux, were obtained from control untransfected muscle fibers.

CELL BIOLOGY

$Ca_V1.1$ when it is expressed by in vivo electroporation into adult muscle fibers (29). Similarly, it has been shown that when GFP was tagged to the N termini of different α1-subunits, including $Ca_V1.1$, and expressed in dysgenic ($Ca_V1.1$ null) myotubes, each GFP-tagged α_{1S} Ca_V subunit exhibited Ca^{2+} channel activity that was indistinguishable from its wild-type untagged counterpart (30). Analogous Cys substitutions have been used previously by others to monitor S4 movements in individual domains VSDs I to IV of $Ca_V1.2$ expressed in oocytes (21), and our approach is based on their procedures.

We electroporated the EGFP-$Ca_V1.1$ L522C construct into flexor digitorum brevis (FDB) muscles of adult mice using standard procedures for in vivo gene transfer in FDB fibers in adult mice (29, 31) (see *SI Appendix* for more details). About 4 to 6 wk later, FDB muscle fibers were isolated and although expression levels and distribution varied between fibers, well-expressing fibers can be identified based on EGFP fluorescence in individual fibers in the whole muscle (Fig. 3 *A*, *Left*). Individual fibers were separated after collagenase treatment and gentle trituration. EGFP fluorescence was observed in isolated FDB fibers using low-magnification fluorescence imaging, (Fig. 3 *A*, *Right*). With higher-magnification confocal imaging, EGFP fluorescence was seen in a repeating striated profile characteristic of the TTs, which are present in mammalian skeletal muscle fibers in a regular pattern consisting of two TTs per 2-μm sarcomere, giving a 1-μm repeat, as seen by high-magnification EGFP confocal fluorescence imaging (Fig. 3 *B*, *Left*: EGFP-$Ca_V1.1$ Cys). Isolated FDB fibers from muscles electroporated with EGFP-$Ca_V1.1$ L522C were then exposed to –SH labeling fluorescent reagent 2-((5 (6)-tetramethyl-rhodamine)carboxylamino)ethyl methanethiosulfonate (TAMRA, 10 μM for 5 min).

During this 5-min exposure, the fibers were repetitively stimulated via remote electrodes in the bath to produce APs at a rate of 50 Hz during 300-ms trains every second for 5 min. The field stimulation evoked-AP depolarization activated the $Ca_V1.1$ voltage sensors, and the resulting S4 movements presumably provide the –SH reactive rhodamine labeling reagent access to the Cys introduced at residue L522C. Imaging the resulting –SH-rhodamine reacted fiber (Fig. 3*B*, TAMRA) (EGFP-$Ca_V1.1$-L522C-rhod, where rhod represents the SH-reactive rhodamine fluorophore covalently attached to the introduced –SH), we found essentially the same TT pattern as for EGFP, but with a bit more "fuzziness," probably due to more diffuse nonspecific staining with the rhodamine –SH reagent (see overlap of EGFP and rhodamine label in Fig. 3 *B*, *Right*). These results establish that we can express Cys-substituted EGFP-$Ca_V1.1$ and fluorescently react the introduced Cys –SH in adult mouse muscle fibers. Even though exogenous $Ca_V1.1$ is present in transfected fibers but not in nontransfected fibers (Fig. 3 *C* and *D*), the transfected fibers do not exhibit any noticeable increase in total expression of $Ca_V1.1$, as judged by the similarity of anti-$Ca_V1.1$ staining in the same pool of transfected and nontransfected fibers (Fig. 3*E*). Thus, our results also show that expression of EGFP-Ca_V.1.1 construct does not modify the overall expression of $Ca_V1.1$ channels in adult muscle fibers (Fig. 3 *C*–*E*), as previously reported (29).

To examine whether the expressed and SH-reactive rhod fluorescently labeled construct (here EGFP-$Ca_V1.1$-L522C-TAMRA) exhibits a change in fluorescence during fiber depolarization, we triggered APs by short (1 ms) electric field stimuli delivered via remote bath electrodes while monitoring the rhod fluorescence using ultrahigh-speed (50 to 100 μs per line) confocal fluorescence line scan imaging (32–36) with the Zeiss LSM-5LIVE system synchronized with the field stimuli. After staining with TAMRA and reducing movement with the myosin-ATPase inhibitor *N*-benzyl-p-toluene sulphonamide (BTS) (37), fluorescence emitted from TAMRA attached to VSDII exhibited a clear early negative-going change in fluorescence in response to a single AP, which decayed back to baseline after the AP (Fig. 4*A*, red trace), as expected for the return of the VSD. Negative-going signals were not detected in TAMRA-stained fibers expressing EGFP-$Ca_V1.1$ without engineered cysteines (Fig. 4*C*). The early negative signals are likely

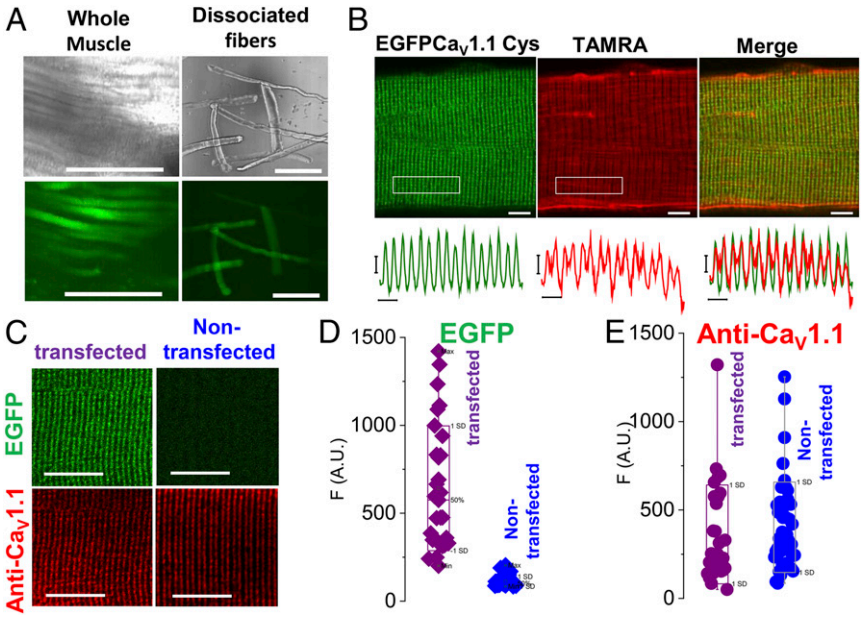

Fig. 3. Expression of Cys engineered $Ca_V1.1$. (*A*) Transmitted and confocal fluorescence images of whole muscle (*Left*) and muscle fibers (*Right*) electroporated with EGFP-$Ca_V1.1$ L522C plasmid (VSDII). (Scale bars, 200 μm.) (*B, Upper*) Confocal images of a muscle fiber expressing EGFP-$Ca_V1.1$ L522C (VSDII) construct (*Left*) and its staining with Cys-reacting fluorescent dye TAMRA (*Center*). (Scale bars, 5 μm.) (*Lower*) Fluorescent profiles of EGFP and TAMRA were analyzed in the boxed regions. (Scale bars, 2 μm.) Merged images (*Right*) show codistribution of both signals. (*C*) EGFP fluorescence (*Upper*) and $Ca_V1.1$ immunolabeling (*Lower*) in a transfected Cys-engineered GFP-$Ca_V1.1$ L522C (VSDII) (*Left*) or a nontransfected fiber (*Right*). (Scale bars, 10 μm.) Box-plot summary for average GFP signal (*D*) and $Ca_V1.1$ immunostaining (*E*) in transfected and nontransfected fibers. No significant difference in $Ca_V1.1$ immunostaining was found between transfected ($n = 29$) and nontransfected fibers ($n = 45$), $P = 0.64$, two sample t test. Whisker indicate minimum and maximum; box delimitation indicates ±SD.

generated by the quenching of Cys-reacting fluorophore when the labeled VSDII moves outward in the membrane (22) during the muscle fiber AP.

Importantly, other fibers expressing the same Cys-engineered VSDII, but stained with the different extracellular labeling reagent tetramethylrhodamine-5-maleimide (TMRM), exhibited a positive-going early fluorescence change in response to a single AP (Fig. 4*B*, red trace). Such opposite-direction signals for TAMRA- and TMRM-stained fibers is consistent with fluorescence signals previously observed in VCF experiments using oocytes expressing $Ca_V1.2$ constructs with analogous Cys substitution in the VSDs (21). For our present studies, the negative-going signal is fortuitously helpful in distinguishing the early TAMRA signal from a later movement signal (Fig. 4*A*, gray trace), which is also minimized by using BTS (Fig. 4*A*, red trace). The similarity of the observed time courses for the two different labels at the same Cys lends credence to the expression, reaction, and monitoring of S4 movement signals from EGFP-$Ca_V1.1$ -L522C during depolarization in muscle fibers. Cys-labeled nontransfected fibers showed movement signals that were eliminated by BTS, but no early dye fluorescence signal in response to an AP (Fig. 4*C*). Our results represent recordings of VSD movements in its native environment in an excitable mammalian cell and recordings of VSD movement in response to an AP in any system.

We next determined the mean time course of the S4 fluorescence change signals for each of the VSDs (I–IV) in $Ca_V1.1$ in different fibers. Importantly, the cysteine substitutions in each of the VSDs as used here in $Ca_V1.1$ (VSDI L159C; VSDII L522C; VSDIII V893C; VSDIV S1231C) had minimal effects on the biophysical profiles of the gating currents and Ca^{2+} currents when compared with EGFP-tagged wild-type counterpart (*SI Appendix*, Figs. S4 and S5 and Tables S1 and S2). Likewise, TAMRA Cys labeling produced negligible effects on the kinetics and voltage-dependence of the gating currents from Cys-modified $Ca_V1.1$ channels (*SI Appendix*, Fig. S6 and Tables S2 and S3). Similarly, neither the morphology and contractility (*SI Appendix*, Fig. S7 and

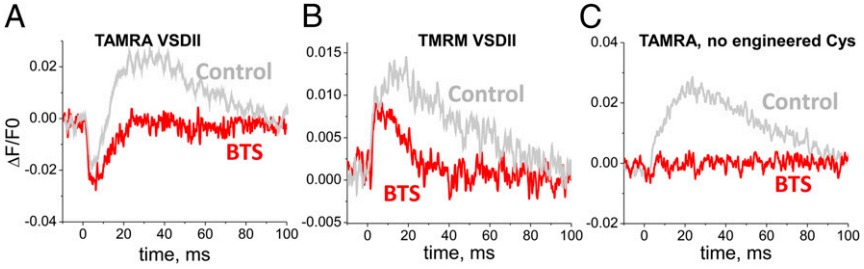

Fig. 4. AP fluorometry of Cys engineered $Ca_V1.1$ with two cysteine reacting dyes attached to VSDII. Exemplar AP-induced fluorometric recordings from a fiber expressing EGFP-$Ca_V1.1$ L522C (VSDII) and stained with TAMRA (*A*) or TMRM (*B*) in control (gray traces) or BTS-added (red traces) recording solution. (*C*) TAMRA signal from a fiber not expressing a Cys-engineered $Ca_V1.1$. No early AP-evoked fluorescence is observed in labeled fibers expressing EGFP-$Ca_V1.1$ without engineered Cys.

Movie S1) nor AP-induced Ca^{2+} transients (*SI Appendix*, Fig. S8) were affected by TAMRA staining and repetitive stimulation (5-min, 300-ms, 50-Hz trains per second) in muscle fibers expressing Cys-engineered $Ca_V1.1$ channels. Charge movement measured in untransfected muscle fibers was also unaffected by TAMRA staining (*SI Appendix*, Fig. S9). The above results indicate that conjugation of cysteines did not alter the biophysical profiles of native or Cys-engineered $Ca_V1.1$ channels. Our results also show that Cys-conjugation and repetitive stimulation did not interfere with the contractile properties or the AP-induced Ca^{2+} transients in fibers expressing Cys-engineered channels.

Time courses of the fluorescence records from the individual fibers for each S4 are presented in *SI Appendix*, Fig. S3. Note that for normalization and comparison the VSD signals are presented as positive-going in Fig. 5 and *SI Appendix*, Fig. S3. Also note that, there is variability of the decay time courses of the fluorescence signals for each of the constructs, presumably due to the variability of remaining nonsuppressed fiber movement, whereas the rising phases are more similar (*SI Appendix*, Fig. S3). The fluorometric signals from the VSDs were likely derived from intrinsic protein rearrangements linked to the S4 domains and not caused by Cys substitutions and Cys-reacting staining (*SI Appendix*, Figs. S4–S9). In Fig. 5 we compare the mean normalized fluorescence change record for each VSD with the normalized trajectories of membrane potential during an APVC, charge movement during an AP, the Ca^{2+} transient for an AP, and the underlying SR Ca^{2+} release rate, measured in a different set of untransfected muscle fibers and repeated in Fig. 5. As expected, the VSD signals occurred after the AP. However, their duration and time to peak were quite prolonged and delayed, respectively, when compared with the electrically measured charge movement during an AP (Fig. 5).

Note that the time course of VSDII accompanied more closely the trajectory of the AP-evoked myoplasmic Ca^{2+} transient (Fig. 5*B*, black trace), whereas rearrangements of VDSs I and IV were slightly more prolonged and VSDIII was even more prolonged (Fig. 5 *A*, *C*, and *D*). All the VSD signals were also much slower and delayed relative to the Ca^{2+} release waveform (Fig. 5, dark green trace). Thus, a considerable fraction of the fluorescence change signal for each VSD occurred after the time of peak Ca^{2+} release, and even more happened after the earlier peak of charge movement during an AP (Fig. 5, dashed lines), and consequently could not directly reflect activation of Ca^{2+} release or charge movement, respectively. Yet, a sizable fraction of the signals for VSDs I, II, and IV, but not VSDIII overlap the rising phase of charge moved (Fig. 5, dashed line indicates time of Q_{max}), and even more for Ca^{2+} release, and thus could reflect voltage-sensor rearrangements and/or Ca^{2+} release activation. Overall, our results unveiled differences in the time courses of $Ca_V1.1$ VSD movements, and in their correlation with the AP, charge movement, Ca^{2+} transient and SR Ca^{2+} release for the four VSDs in their native environment, supporting the view that VSDs operate differentially and could contribute to specific aspects of $Ca_V1.1$ and ECC gating.

Discussion

In this paper we report two major findings. First, we present measurements of the voltage-sensor intramembrane charge movement in response to the AP waveform, the major physiological signal for information transmission in excitable cells. Much of the existing experimental information on voltage-sensing mechanisms of muscle contraction relates to their responses to voltage-clamp steps and not to APs. Early reports suggested an involvement of some or all of the charge movement (i.e., Qβ vs. Qγ) in triggering skeletal muscle ECC (38–42). To our knowledge, this is a description of voltage-sensor movement during an AP in any cell or expression system, as predicted by Hodgkin and Huxley (43) and in agreement with previous models (44, 45), is unique. The charge movement coupled to ECC is attributable entirely to $Ca_V1.1$ (42), with all four VSDs contributing in an as yet to be determined proportion to the overall recorded charge movement.

Second, we attempted to separate the individual contributions of each VSD to activation in response to an AP. We expressed Cys-engineered $Ca_V1.1$ channels in adult muscle fibers, with each construct having a Cys residue inserted just extracellular to the S4 α-helix in one of the four VSDs, stained the fibers with Cys-reactive fluorophore, and identified a small optical signal related to signaling by each of the VSDs during a single AP. Both observations were obtained using fully differentiated and mature skeletal muscle fibers in response to the normal physiological signal of a single muscle fiber AP. VCF has provided extensive information regarding intramolecular rearrangements in the VSDs of voltage-sensitive membrane channels during membrane depolarization, first for K^+ (22, 46, 47) and Na^+ channels (19, 48), and more recently for the cardiac Ca^{2+} channel, $Ca_V1.2$ (21, 49). Our study represents a study of ion channel VSD activation in its native system. Such characterization is particularly important in skeletal muscle as $Ca_V1.1$ not only senses membrane voltage, but also communicates the ECC signal to RyR1 via bidirectional conformational coupling (50, 51). Therefore, the study of the roles of VSDs in skeletal muscle ECC, requires the presence of both $Ca_V1.1$ and RyR1.

Voltage-clamping using the AP waveform as the clamp command has been used previously to determine the time course of various membrane currents during the AP in several excitable cell types (24, 25). Here, we eliminate current through all membrane channels, but instead of using voltage steps as command pulses, we use the AP waveform recorded during a propagated AP as the

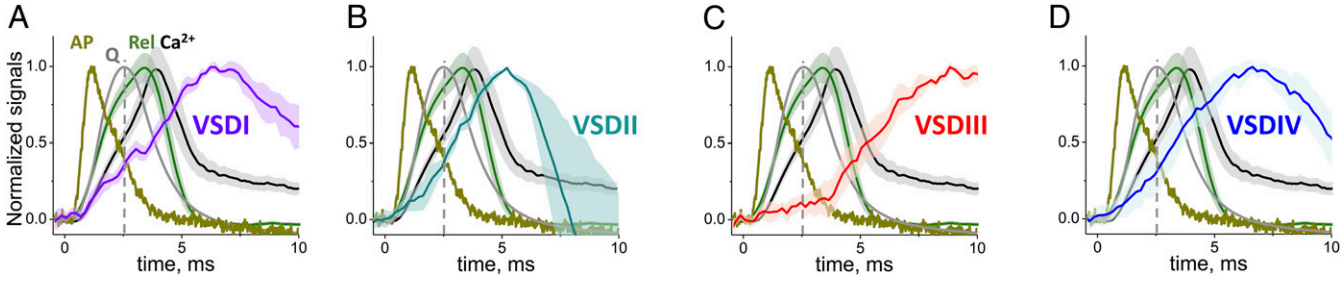

Fig. 5. AP-induced fluorescence response for each $Ca_V1.1$ VSD. (*A–D*) Normalized traces of average AP-induced fluorometric records (n = 3 to 5) of each of the individual VSDs (as indicated) in relation to optically measured AP (dark yellow trace), APVC-elicited charge movement (Q; gray, data from Fig. 2*I*) and AP-evoked fluo-4 Ca^{2+} transient (Ca^{2+}; black) and corresponding Ca^{2+} release flux waveform (Rel; green trace, data from Fig. 2*I*). VSDs, Ca^{2+} transient and Ca^{2+} release signals were assessed in different sets of fibers and are presented ±SEM. AP, Q, Ca^{2+} transients, and derived Ca^{2+} release flux, were obtained from control untransfected muscle fibers (n = 11 to 12). TAMRA signals are shown as $-\Delta F/F0$. Peak $-\Delta F/F0$ responses for all VSDs ranged from 0.008 to 0.03 (a.u.). AP, Ca^{2+} transient, VSDs fluorescent signals were elicited by field stimulation (1 ms, 20 V) at time 0. Vertical dashed lines indicate time for $Q = Q_{max}$.

voltage-clamp command signal. With these conditions, we find that the peak amount of charge moved by the VSD domains during the AP waveform is about 65% of Q_{max}, the maximum amount of charge movement available, which was measured by a step depolarization to +20 mV, a voltage where charge movement is typically maximum. Thus, in principle, a large fraction of the RyR1 SR Ca^{2+} release channels coupled to the $Ca_V1.1$s could be activated by a single AP.

In the present study, we engineered $Ca_V1.1$ by introducing a Cys residue near one of the S4 helices for each of the VSDs and carry out the expression, fluorescent staining, AP, AP-evoked charge movement, AP-evoked Ca^{2+} transient measurements, and estimated underlying Ca^{2+} release flux in adult mouse skeletal muscle fibers. Fluorometric signals in response to a single AP were obtained after expression of each of the Cys-engineered $Ca_V1.1$s and subsequent fiber staining with a Cys-reactive fluorophore, but not in similarly fluorescently stained fibers that did not express mutant channels. However, the fluorescence change signals for each of the four VSDs of $Ca_V1.1$ were delayed compared with the electrically measured total charge movement for a voltage-clamped AP. This observation raises the possibility of a temporal delay between the actual charge moved within the membrane across the membrane field and the secondary conformational change of regions of the VSD as fluorescently labeled here that are just extracellular to the membrane and almost certainly outside the membrane electric field. In this regard, Cys substitution and fluorophore reaction at the analogous site in $K_V1.2/2.1$ chimera in *Xenopus* oocytes were similarly delayed compared with the signal from an artificial fluorescent amino acid substituted near the cytosolic end of S1 (46) in close proximity to the gating charge that is displaced. The structural similarity between K_V channels and $Ca_V1.1$ suggests that other locations near the cytoplasmic end of the voltage sensor may give less-delayed VSD signals than the locations just proximal to S4 labeled here, and thus warrant exploration in the future.

In other voltage-gated channel family members, individual VSDs appear to be differentially involved in specific aspects of channel gating (18–21, 52). Strong evidence in favor for a differential role of each VSD in $Ca_V1.1$ channel operation using chimeric studies and alternative splicing of VSDs of $Ca_V1.1$ suggests that VSDs I and IV control the activation kinetics and voltage-dependence of Ca^{2+} channel current, respectively (53–56), and it has been hypothesized that VSDII and VSDIII could be primarily involved in ECC (53, 57). VSDII and VSDIII are good candidates for ECC activation via intramolecular and intermolecular arrangements. The VSDII S4-charged transmembrane helix is positioned three transmembrane segments away from the I-II loop (Fig. 1*A*), an important region for interaction with the auxiliary β_{1a}-subunit, which is also essential for ECC (58–60). However, the functional impact of the I-II/β_{1a} interaction is still not defined. VSDIII is also just two transmembrane segments away from the intracellular II-III loop, another region regarded as critical for $Ca_V1.1$–RyR1 coupling (61–63).

Our study is an attempt to correlate the AP-induced activation of individual VSDs with the time course of charge movement and Ca^{2+} transient and Ca^{2+} release in fully differentiated skeletal muscle fibers. Here we report that VSD signals were slower than the AP-induced charge movement, indicating that the fluorometric signals likely represent slower conformational changes than those producing the bulk of charge movement. However, the early activation component of VSDs I, II, and IV accompanied the time course of the charge movement and Ca^{2+} release initiated by an AP, suggesting that S4 movement of these VSDs could be linked to the activation of RyR1 channels. For the particular physiological voltage waveform of the muscle fiber AP, none of the present $\Delta F(t)$ signals from any of the VSDs is fast enough to correspond directly to the electrically measured $Q(t)$. Furthermore, no summation of the scaled $\Delta F(t)$ for the four individual VSDs can give the $Q(t)$ because each of the $\Delta F(t)$ signals is slower than $Q(t)$. Thus, one or more of the $\Delta F(t)$ signals is missing an earlier component corresponding to the putative early movement of one or more of the VSDs. Further work is needed to identify such an early fluorescence conformational change signal related to the electrically detected VSD movements.

While the detailed role of each individual VSDs in ECC remains unclear, our work introduces the use of AP fluorometry to study the activation of $Ca_V1.1$ VSDs and RyR1 Ca^{2+} release in its native environment and physiological stimuli. Yet, additional work is needed to address various remaining unanswered questions. For example, are all charged residues in S4 critical for controlling Ca^{2+} release? How far and how exactly do each charged residue in S4 translocate? Which and how many VSDs in the tetrads, arrays of four $Ca_V1.1$ channels aligned with the four subunits of coupled RyR1 (59, 64), are required to activate RyR1? One salient limitation of our study is that the charge movement, $Ca_V1.1$ VSD fluorometric signals and Ca^{2+} transients were not evaluated in the same fibers. Future studies of simultaneous measurements of charge movement, Ca^{2+} transients, and VSD fluorometric signals using AP fluorometry and step-depolarizations VCF in Cys-labeled and unnatural fluorescent amino acid-engineered Cav1.1 channels, which may permit the tracking of buried transmembranal or membrane-facing residues in S4, will further our understating of the VSDs in $Ca_V1.1$ and their contribution to ECC in muscle fibers.

Materials and Methods

A plasmid coding for the N-terminally EGFP-tagged of the full-length cDNA coding for the wild-type α_{1S} subunit of the $Ca_V1.1$ from rabbit skeletal (28) muscle was used to develop cysteine-engineered S4 for each VSD. All constructs were expressed in FDBs of live 4-wk-old mice using in vivo gene transfer, as previously described (27, 28). Experimental protocols were approved by the University of Maryland Institutional Animal Care and Use Committee. AP-induced rearrangements of each VSD were monitored using AP-elicited fluorometry and ultra-high speed (20 to 200 μs per line) laser confocal microscopy. For comprehensive details see *SI Appendix, Expanded Materials and Methods*.

Data Availability. All study data are included in the article and supporting information.

ACKNOWLEDGMENTS. We thank Dr. J. Vergara (University of California, Los Angeles) for sharing the EGFP-$Ca_V1.1$ (rabbit) wild-type plasmid and Dr. B. E. Flucher (Medizinische Universität Innsbruck) for providing the GLT (dysGenic *L*ine transfected with the large *T* antigen) cells. This work was supported by NIH Grants R37AR055099 and R01AR075726 (to M.F.S), R01NS103777 (to R.A.B), and T32AR007592 (to Q.B.).

1. E. Rios, G. Brum, Involvement of dihydropyridine receptors in excitation-contraction coupling in skeletal muscle. *Nature* **325**, 717–720 (1987).
2. M. F. Schneider, W. K. Chandler, Voltage dependent charge movement of skeletal muscle: A possible step in excitation-contraction coupling. *Nature* **242**, 244–246 (1973).
3. T. Imagawa, J. S. Smith, R. Coronado, K. P. Campbell, Purified ryanodine receptor from skeletal muscle sarcoplasmic reticulum is the Ca^{2+}-permeable pore of the calcium release channel. *J. Biol. Chem.* **262**, 16636–16643 (1987).
4. G. Meissner, E. Darling, J. Eveleth, Kinetics of rapid Ca^{2+} release by sarcoplasmic reticulum. Effects of Ca^{2+}, Mg^{2+}, and adenine nucleotides. *Biochemistry* **25**, 236–244 (1986).
5. A. Sandow, Excitation-contraction coupling in muscular response. *Yale J. Biol. Med.* **25**, 176–201 (1952).
6. P. R. Stanfield, A calcium dependent inward current in frog skeletal muscle fibres. *Pflugers Arch.* **368**, 267–270 (1977).
7. R. A. Bannister, K. G. Beam, Ca(V)1.1: The atypical prototypical voltage-gated Ca^{2+} channel. *Biochim. Biophys. Acta* **1828**, 1587–1597 (2013).
8. C. S. Lee *et al*., Ca(2+) permeation and/or binding to CaV1.1 fine-tunes skeletal muscle Ca(2+) signaling to sustain muscle function. *Skelet. Muscle* **5**, 4 (2015).
9. A. Dayal *et al*., The Ca^{2+} influx through the mammalian skeletal muscle dihydropyridine receptor is irrelevant for muscle performance. *Nat. Commun.* **8**, 475 (2017).

10. R. H. Adrian, L. L. Costantin, L. D. Peachey, Radial spread of contraction in frog muscle fibres. *J. Physiol.* **204**, 231–257 (1969).
11. W. A. Catterall, Structure and regulation of voltage-gated Ca^{2+} channels. *Annu. Rev. Cell Dev. Biol.* **16**, 521–555 (2000).
12. J. Wu *et al*., Structure of the voltage-gated calcium channel Ca(v)1.1 at 3.6 Å resolution. *Nature* **537**, 191–196 (2016).
13. T. Tanabe *et al*., Primary structure of the receptor for calcium channel blockers from skeletal muscle. *Nature* **328**, 313–318 (1987).
14. S. K. Aggarwal, R. MacKinnon, Contribution of the S4 segment to gating charge in the Shaker K^+ channel. *Neuron* **16**, 1169–1177 (1996).
15. F. Bezanilla, The voltage sensor in voltage-dependent ion channels. *Physiol. Rev.* **80**, 555–592 (2000).
16. S. A. Seoh, D. Sigg, D. M. Papazian, F. Bezanilla, Voltage-sensing residues in the S2 and S4 segments of the Shaker K^+ channel. *Neuron* **16**, 1159–1167 (1996).
17. N. Yang, R. Horn, Evidence for voltage-dependent S4 movement in sodium channels. *Neuron* **15**, 213–218 (1995).
18. A. Cha, P. C. Ruben, A. L. George Jr, E. Fujimoto, F. Bezanilla, Voltage sensors in domains III and IV, but not I and II, are immobilized by Na^+ channel fast inactivation. *Neuron* **22**, 73–87 (1999).
19. B. Chanda, F. Bezanilla, Tracking voltage-dependent conformational changes in skeletal muscle sodium channel during activation. *J. Gen. Physiol.* **120**, 629–645 (2002).
20. Y. Muroi, M. Arcisio-Miranda, S. Chowdhury, B. Chanda, Molecular determinants of coupling between the domain III voltage sensor and pore of a sodium channel. *Nat. Struct. Mol. Biol.* **17**, 230–237 (2010).
21. A. Pantazis, N. Savalli, D. Sigg, A. Neely, R. Olcese, Functional heterogeneity of the four voltage sensors of a human L-type calcium channel. *Proc. Natl. Acad. Sci. U.S.A.* **111**, 18381–18386 (2014).
22. L. M. Mannuzzu, M. M. Moronne, E. Y. Isacoff, Direct physical measure of conformational rearrangement underlying potassium channel gating. *Science* **271**, 213–216 (1996).
23. M. F. Schneider, Membrane charge movement and depolarization-contraction coupling. *Annu. Rev. Physiol.* **43**, 507–517 (1981).
24. R. Llinás, M. Sugimori, S. M. Simon, Transmission by presynaptic spike-like depolarization in the squid giant synapse. *Proc. Natl. Acad. Sci. U.S.A.* **79**, 2415–2419 (1982).
25. A. Taddese, B. P. Bean, Subthreshold sodium current from rapidly inactivating sodium channels drives spontaneous firing of tuberomammillary neurons. *Neuron* **33**, 587–600 (2002).
26. C. M. Armstrong, F. Bezanilla, Charge movement associated with the opening and closing of the activation gates of the Na channels. *J. Gen. Physiol.* **63**, 533–552 (1974).
27. B. L. Prosser, E. O. Hernández-Ochoa, D. B. Zimmer, M. F. Schneider, The Qgamma component of intra-membrane charge movement is present in mammalian muscle fibres, but suppressed in the absence of S100A1. *J. Physiol.* **587**, 4523–4541 (2009).
28. M. DiFranco, M. Quinonez, J. Capote, J. Vergara, DNA transfection of mammalian skeletal muscles using in vivo electroporation. *J. Vis. Exp.* **32**, 1520 (2009).
29. M. DiFranco, P. Tran, M. Quiñonez, J. L. Vergara, Functional expression of transgenic 1sDHPR channels in adult mammalian skeletal muscle fibres. *J. Physiol.* **589**, 1421–1442 (2011).
30. M. Grabner, R. T. Dirksen, K. G. Beam, Tagging with green fluorescent protein reveals a distinct subcellular distribution of L-type and non-L-type Ca^{2+} channels expressed in dysgenic myotubes. *Proc. Natl. Acad. Sci. U.S.A.* **95**, 1903–1908 (1998).
31. T. Shen *et al*., DNA binding sites target nuclear NFATc1 to heterochromatin regions in adult skeletal muscle fibers. *Histochem. Cell Biol.* **134**, 387–402 (2010).
32. E. O. Hernández-Ochoa, Q. Banks, M. F. Schneider, Acute elevated glucose promotes abnormal action potential-induced Ca^{2+} transients in cultured skeletal muscle dibers. *J. Diabetes Res.* **2017**, 1509048 (2017).
33. E. O. Hernández-Ochoa, M. Contreras, Z. Cseresnyés, M. F. Schneider, Ca^{2+} signal summation and NFATc1 nuclear translocation in sympathetic ganglion neurons during repetitive action potentials. *Cell Calcium* **41**, 559–571 (2007).
34. E. O. Hernández-Ochoa *et al*., Loss of S100A1 expression leads to Ca^{2+} release potentiation in mutant mice with disrupted CaM and S100A1 binding to CaMBD2 of RyR1. *Physiol. Rep.* **6**, e13822 (2018).
35. E. O. Hernández-Ochoa, S. J. P. Pratt, K. P. Garcia-Pelagio, M. F. Schneider, R. M. Lovering, Disruption of action potential and calcium signaling properties in malformed myofibers from dystrophin-deficient mice. *Physiol. Rep.* **3**, e12366 (2015).
36. E. O. Hernández-Ochoa, C. Vanegas, S. R. Iyer, R. M. Lovering, M. F. Schneider, Alternating bipolar field stimulation identifies muscle fibers with defective excitability but maintained local Ca(2+) signals and contraction. *Skelet. Muscle* **6**, 6 (2016).
37. J. Bruton, G. J. Pinniger, J. Lännergren, H. Westerblad, The effects of the myosin-II inhibitor N-benzyl-p-toluene sulphonamide on fatigue in mouse single intact toe muscle fibres. *Acta Physiol. (Oxf.)* **186**, 59–66 (2006).
38. G. Brum, E. Rios, Intramembrane charge movement in frog skeletal muscle fibres. Properties of charge 2. *J. Physiol.* **387**, 489–517 (1987).
39. P. Horowicz, M. F. Schneider, Membrane charge moved at contraction thresholds in skeletal muscle fibres. *J. Physiol.* **314**, 595–633 (1981).
40. C. L. Huang, Experimental analysis of alternative models of charge movement in frog skeletal muscle. *J. Physiol.* **336**, 527–543 (1983).
41. C. L. Huang, Intramembrane charge movements in skeletal muscle. *Physiol. Rev.* **68**, 1197–47 (1988).
42. E. Ríos, G. Pizarro, Voltage sensor of excitation-contraction coupling in skeletal muscle. *Physiol. Rev.* **71**, 849–908 (1991).
43. A. L. Hodgkin, A. F. Huxley, A quantitative description of membrane current and its application to conduction and excitation in nerve. *J. Physiol.* **117**, 500–544 (1952).
44. R. H. Adrian, L. D. Peachey, Reconstruction of the action potential of frog sartorius muscle. *J. Physiol.* **235**, 103–131 (1973).
45. C. L. Huang, L. D. Peachey, A reconstruction of charge movement during the action potential in frog skeletal muscle. *Biophys. J.* **61**, 1133–1146 (1992).
46. T. Kalstrup, R. Blunck, Dynamics of internal pore opening in K(V) channels probed by a fluorescent unnatural amino acid. *Proc. Natl. Acad. Sci. U.S.A.* **110**, 8272–8277 (2013).
47. T. Kalstrup, R. Blunck, S4-S5 linker movement during activation and inactivation in voltage-gated K^+ channels. *Proc. Natl. Acad. Sci. U.S.A.* **115**, E6751–E6759 (2018).
48. Z. Varga *et al*., Direct measurement of cardiac Na^+ channel conformations reveals molecular pathologies of inherited mutations. *Circ. Arrhythm. Electrophysiol.* **8**, 1228–1239 (2015).
49. N. Savalli *et al*., The $\alpha 2\delta$-1 subunit remodels CaV1.2 voltage sensors and allows Ca^{2+} influx at physiological membrane potentials. *J. Gen. Physiol.* **148**, 147–159 (2016).
50. J. Nakai *et al*., Enhanced dihydropyridine receptor channel activity in the presence of ryanodine receptor. *Nature* **380**, 72–75 (1996).
51. D. C. Sheridan *et al*., Bidirectional signaling between calcium channels of skeletal muscle requires multiple direct and indirect interactions. *Proc. Natl. Acad. Sci. U.S.A.* **103**, 19760–19765 (2006).
52. D. L. Capes, M. P. Goldschen-Ohm, M. Arcisio-Miranda, F. Bezanilla, B. Chanda, Domain IV voltage-sensor movement is both sufficient and rate limiting for fast inactivation in sodium channels. *J. Gen. Physiol.* **142**, 101–112 (2013).
53. B. E. Flucher, Specific contributions of the four voltage-sensing domains in L-type calcium channels to gating and modulation. *J. Gen. Physiol.* **148**, 91–95 (2016).
54. P. Tuluc, B. Benedetti, P. Coste de Bagneaux, M. Grabner, B. E. Flucher, Two distinct voltage-sensing domains control voltage sensitivity and kinetics of current activation in $Ca_V1.1$ calcium channels. *J. Gen. Physiol.* **147**, 437–449 (2016).
55. P. Tuluc, B. E. Flucher, Divergent biophysical properties, gating mechanisms, and possible functions of the two skeletal muscle Ca(V)1.1 calcium channel splice variants. *J. Muscle Res. Cell Motil.* **32**, 249–256 (2011).
56. P. Tuluc, V. Yarov-Yarovoy, B. Benedetti, B. E. Flucher, Molecular interactions in the voltage sensor controlling gating properties of CaV calcium channels. *Structure* **24**, 261–271 (2016).
57. E. O. Hernández-Ochoa, M. F. Schneider, Voltage sensing mechanism in skeletal muscle excitation-contraction coupling: Coming of age or midlife crisis? *Skelet. Muscle* **8**, 22 (2018).
58. R. G. Gregg *et al*., Absence of the beta subunit (cchb1) of the skeletal muscle dihydropyridine receptor alters expression of the alpha 1 subunit and eliminates excitation-contraction coupling. *Proc. Natl. Acad. Sci. U.S.A.* **93**, 13961–13966 (1996).
59. J. Schredelseker *et al*., The beta 1a subunit is essential for the assembly of dihydropyridine-receptor arrays in skeletal muscle. *Proc. Natl. Acad. Sci. U.S.A.* **102**, 17219–17224 (2005).
60. C. Strube, M. Beurg, P. A. Powers, R. G. Gregg, R. Coronado, Reduced Ca^{2+} current, charge movement, and absence of Ca^{2+} transients in skeletal muscle deficient in dihydropyridine receptor beta 1 subunit. *Biophys. J.* **71**, 2531–2543 (1996).
61. G. Kugler, R. G. Weiss, B. E. Flucher, M. Grabner, Structural requirements of the dihydropyridine receptor alpha1S II-III loop for skeletal-type excitation-contraction coupling. *J. Biol. Chem.* **279**, 4721–4728 (2004).
62. J. Nakai, T. Tanabe, T. Konno, B. Adams, K. G. Beam, Localization in the II-III loop of the dihydropyridine receptor of a sequence critical for excitation-contraction coupling. *J. Biol. Chem.* **273**, 24983–24986 (1998).
63. T. Tanabe, K. G. Beam, B. A. Adams, T. Niidome, S. Numa, Regions of the skeletal muscle dihydropyridine receptor critical for excitation-contraction coupling. *Nature* **346**, 567–569 (1990).
64. B. A. Block, T. Imagawa, K. P. Campbell, C. Franzini-Armstrong, Structural evidence for direct interaction between the molecular components of the transverse tubule/sarcoplasmic reticulum junction in skeletal muscle. *J. Cell Biol.* **107**, 2587–2600 (1988).